Spatial Kinematic Analysis of Threaded Fastener Assembly

Stephen Wiedmann
Southwest Research Institute,
6220 Culebra Rd.,
San Antonio, TX 78238
e-mail: swiedmann@swri.org

Bob Sturges
Industrial & Systems Engineering,
Virginia Tech,
100 Durham Hall,
Blacksburg, VA 24061
e-mail: sturges@vt.edu

Compliant mechanisms for rigid part mating exist for prismatic geometries. A few instances are known of mechanisms to assemble screw threads. A comprehensive solution to this essentially geometric problem comprises at least three parts: parametric equations for nut and bolt contact in the critical starting phase of assembly, the possible space of motions between these parts during this phase, and the design space of compliant devices which accomplish the desired motions in the presence of friction and positional uncertainty. This work concentrates on the second part in which the threaded pair is modeled numerically, and contact tests are automated through software. Tessellated solid models were used during three-dimensional collision analysis to enumerate the approximate location of the initial contact point. The advent of a second contact point presented a more constrained contact state. Thus, the bolt is rotated about a vector defined by the initial two contact points until a third contact location was found. By analyzing the depth of intersection of the bolt into the nut as well as the vertical movement of the origin of the bolt reference frame, we determined that there are three types of contacts states present: unstable two-point, quasi-stable two-point, stable three point. The space of possible motions is bounded by these end conditions which will differ in detail depending upon the starting orientations. We investigated all potential orientations which obtain from a discretization of the roll, pitch, and yaw uncertainties, each of which has its own set of contact points. From this exhaustive examination, a full contact state history was determined, which lays the foundation for the design space of either compliant mechanisms or intelligent sensor-rich controls. [DOI: 10.1115/1.2114909]

1 Introduction

Modern manufacturing is faced with reduced production times and smaller volumes. A promising approach with some current application employs compliant mechanisms or sensor-effector algorithms for rigid part mating exist for prismatic geometries. Since threaded fasteners represent a more labor- and effort-intensive class of assemblies, significant economic drivers exist for improvements with this geometry. A few instances are known of mechanisms to assemble threaded pairs, but generalizations of these inventions have not been made. A comprehensive solution to this essentially geometric problem comprises at least three parts: parametric equations for nut and bolt contact in the critical starting phase of assembly, the possible space of motions between these parts during this phase, and the design space of compliant devices which accomplish the desired motions in the presence of friction and positional uncertainty. This work concentrates on the second part, focusing the nature of contact between a fine-pitched bolt and nut during thread mating when the respective axes are in a skewed relationship to each other. Our ultimate goal is to develop the theory necessary to adapt the compliances needed for passive assembly, for example, the spatial remote center of compliance (RCC) reported by Sturges and Laowattana [1,2].

Our approach is to develop a complete network of contact states that determine the path of successful assembly based on static load relations and failure modes. Here, contact states are the collection of contacts between two parts at each moment during an assembly operation. Failure modes are identified as either jamming, where the applied forces are out of proportion with the contact state no longer permitting assembly, or as wedging, where the contact forces deform the parts and assembly is not possible without reorienting [3].

A constrained three-dimensional analysis was previously completed [4] to provide some insight into how the contacts between a bolt and nut behave during the starting phase of counterclockwise rotation of the bolt. It did not provide the opportunity to analyze the potential for out-of-plane contacts. By modeling the assembly problem in three dimensions, one will be able to determine if any out-of-plane contacts exist. We begin by assuming that the bolt will obtain an out-of-plane contact once it achieves stability, which is defined as three distinct contact points. We also assume that the action follows a minimization of the virtual work done on an unbiased elastic structure, such as an RCC. The following steps predict the path that the bolt will take to obtain stability:

1. Initial contact at predefined spatial orientation.
2. Rotation about a vector tangent to the surface of the nut at the initial contact point until the second contact is made.
3. Rotation about a pivot axis defined by the two contact points until a third contact is obtained.

The direction of rotation at the initial contact point will be negative to ensure that the bolt will rotate in the direction that corrects its spatial orientation. The direction of rotation about the pivot axis will vary depending on the location of the two contact points. While our approach to assembly is through the application of engineered compliances, our results also lay the foundation for algorithmic, sensor-driven methods for automatic assembly.

2 Literature Review

Manufacturers with low volume contracts of moderately difficult assembly operations greatly benefit from innate human dexterity. From an early age a human being has the ability to put simple objects together. However, such assembly tasks in modern assembly lines are tedious slow, and expensive. Potential assembly failures arise due to human error that may be attributed to many consecutive hours of repetitive tasks. Though operator rotation throughout the shift is one way to reduce assembly failure, it still does not provide a high quality cost-effective solution to the assembly of large volume contracts.

Contributed by the Reliability, Stress Analysis and Failure Prevention of ASME for publication in the JOURNAL OF MECHANICAL DESIGN. Manuscript received May 18, 2004; final manuscript received April 26, 2005. Assoc. Editor: Erol Sancaktar.

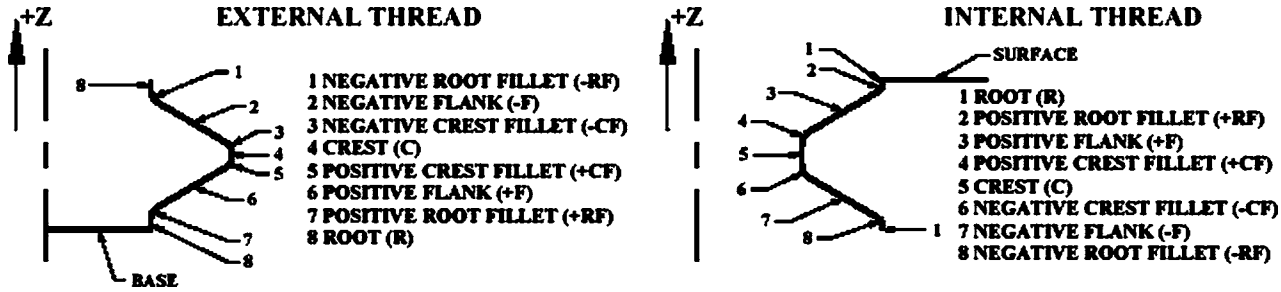

Fig. 1 Internal and external thread profiles

Although the need to be more productive is receiving current headlines, Russian researchers first considered the actual problem of automatic assembly in the 1960s. Though the motivation for these studies was not completely identified, they did provide the groundwork for others once the documents were "edited" and translated. In one study, the author proposed sending a peg on a predescribed search pattern [5]. Threaded fastener insertion is a ubiquitous assembly primitive that has faced some scrutiny in the literature. It was first considered by Blaer [6], who found that in order to assemble threaded parts automatically; the bolt must be centered in the nut and supported by a longitudinal force before rotation of the bolt can begin. More recent work by Nicholson & Fearing [7,8] explores compliant control with a simplified thread model and ideal controller models, both in the quasi-static and dynamic configurations. Their results are empirical and do not predict contact states for reasonably large positioning errors. In a practical implementation of algorithmic correction of positional uncertainty, Diftler [9] relies on measurement and precise servo control to locate the bolt drop action.

Whitney [10] identifies several methods to aid automatic bolt insertion. Several bolt tip shapes are discussed, and the "turn backwards first" method is also mentioned. The prior work [4,11] examined in detail the geometry of this phase of fastener mating.

3 Screw Thread Definitions

The internal and external threads are defined by the American National Standard for Unified Screw Threads [12]. Fillet radii bound the crest and root in order to approximate an actual manufactured thread.

The bolt (or external thread) is made up of nine regions, as shown in Fig. 1 above. The flank is defined as positive if the radius of the bolt increases when measured in the positive azimuth (+*Z*) direction. Likewise, the flank is defined as negative if the radius of the bolt decreases in the positive azimuth direction. This logic is identical for the crest fillet and the root fillet. In addition to these regions the bolt has constant radius surfaces defined as the crest and the root. The ninth, and final, region is known as the base, since the bottom of the bolt completes a surface region and has the potential to become involved during contact.

The nut follows a similar definition, however, due to the nature of an internal thread, the value of the radius is a maximum at the root and a minimum at the crest as measured from the nut azimuth axis. The designation of positive or negative as applied to the flank, crest fillet, and root fillet of the nut follows the same definition as provided for the bolt. The ninth region is known as the surface, and like the bolt, it completes the surface region of the nut that has the potential to come into contact. The top of the bolt and the bottom of the nut are not included here because these regions will not come into contact once the position and orientation errors are introduced.

The pitch of a thread is defined as the vertical change of the thread per one revolution. It provides a threaded assembly the ability to mesh. In order for two threaded parts to mate, the pitch of each must be the same, or the parts will wedge together and become damaged. The amount of vertical change can be calculated with the following equation:

$$z = \frac{p\theta}{2\pi} \quad 0 \leqslant \theta \leqslant 2\pi. \tag{1}$$

Here, p is the pitch in inches (or millimeters) and θ is the angular location in radians. Note that any profile, such as the external thread, which is helically swept, will repeat itself after one full revolution about the azimuth axis.

4 Numerical Contact Analysis

The numerical contact analysis here assumes the Unified Screw Thread standard. For other thread forms, e.g., Acme and Whitworth standards, the values of the constant parameters will differ, especially the flank angles, which are shown here at 60 deg. To use the electrical lamp screws, root, and crest fillet radii would effectively obviate the flank angles resulting in simpler models, not treated here. In order to show that the bolt follows this contact path, a supervisory code was written to isolate the contacts as they occurred in space. To facilitate the detection of these contacts, a software library, known as RAPID [13], was used to determine contact locations between two solid bodies given some initial orientation in space. RAPID required the input of a solid model in a tessellated form. This meant that the bolt and nut must be modeled through solid modeling software, tessellated, and exported into a binary data file. A solid modeler, PRO/ENGINEER release 19, was used to create the images of one pitch of the bolt and nut thread (#1/4-20 UNC). For the contact analysis between the bolt and nut, the best tessellation was desired, so that the minimum values of chord height (1.0×10^{-4}) and angle control (0.5) were chosen for both the nut and bolt. The bolt was made hollow, and the nut was cut out of a 16-sided polygon to reduce the size of triangles that appeared on the top and bottom surfaces of the bolt and nut. This produced a model that deviated from the true surface by a few millionths of an inch, which is within the surface noise of a real threaded part (Fig. 2).

4.1 Contact Location Methodology. Given two intersecting triangles in space, one can locate the approximate coordinates of the contact point at the moment the intersection occurs. Knowing that each triangle defines a plane in space and having nonparallel planes, there will be a line that results from the intersection of the two planes. Now, the vertices of the triangle define three intersecting lines that bound one another and form a triangle in space.

Hence, given two intersecting triangles, one can determine the equation of the plane that each triangle defines via its vertices. From this, the equation of the line resulting from the intersection of the two planes can be derived. Now, the line can be reduced to a line segment by determining where it intersects the sides of the bolt triangle. The bolt triangle is chosen here, because in the tessellation of the solid model it is generally smaller than the nut triangle, and therefore would be more accurate in locating the

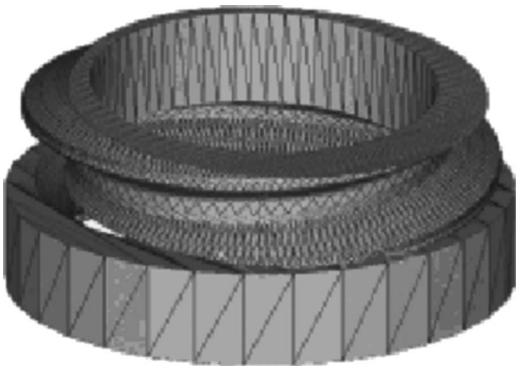

Fig. 2 Tessellated solid model—bolt and nut

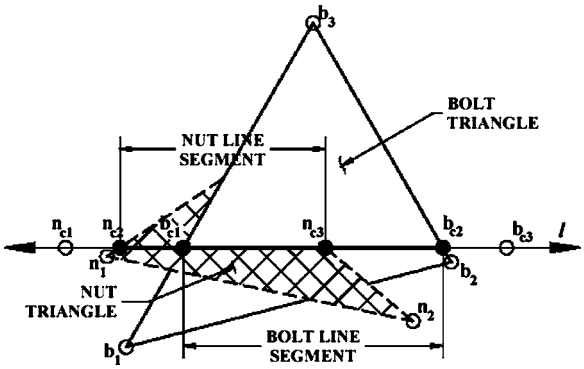

Fig. 4 Endpoints of intersecting line segment

contact point. At this point the boundary of the nut triangle is analyzed to see what part of the line segment is included in the plane bounded by the sides of the nut triangle.

Part of the line segment that lies in the plane of the bolt will intersect at least one of the sides of the nut triangle. Vectors are drawn from the intersecting points in the bolt plane towards the intersecting points in the nut plane. The magnitudes of these vectors are analyzed to determine the appropriate end points of the line segment. Finally, the midpoint of the line segment is taken as the estimated contact point for that contact pair. This process is repeated for each set of contacts and all of the midpoints are summed and averaged in order to produce the approximate contact point. Ideally, the smaller number of contact pairs the better the approximation. The number of triangles in the tessellated model determines the accuracy of this result. For our purposes, by moving the bolt down in steps of 1 instead of 100 μin., we are able to reduce the maximum variation of the calculated contact point by an average of 0.0025 in. The following section details the mathematics involved in the contact point calculation.

4.2 Contact Location Derivation. Currently, we know the symmetric equation of the line defined by a single contact pair. However, multiple contact pairs are involved in a theoretical contact location, since the surface of the bolt will intersect the surface of the nut to some degree thereby increasing the number of contacting triangle pairs. If each contact pair is considered, then how does one determine where the actual contact point occurred? The following algorithm will be presented to approximate the contact location.

Ideally, we are interested in the segment of the line bounded by the plane of the bolt and nut triangle. In fact, both planes must share the line segment because the plane of the bolt and nut defined it. However, the nut triangle may not fully intersect the bolt triangle, as it has the potential to intersect the bolt triangle in four ways (Fig. 3).

Note that in the fourth case, the nut triangle does not actually intersect the bolt triangle, but it has the potential to be returned as a contact pair by RAPID. This is due to the internal accuracy of the collision detection library and cannot be avoided. Hence, the contact location algorithm will check for this special case and only use the line segment defined by the bolt triangle. For the remaining types, the portion of the infinite line that is actually involved with the intersection of the bolt and nut triangle will be used to locate the contact point. The approximate location of the contact point will be the average of the sum of the midpoints for each line segment. Hence, if there are ten contact pairs involved (that fall within the four valid intersection types above), then there will be ten midpoints that will be averaged to define one contact point. The process of enumerating the line segment helps eliminate potential error associated with triangle size. For instance, if the triangles are large, then the line segment bounded by just the bolt triangle will be large, subsequently creating error when calculating the midpoint. However, the length of the line segment can be reduced by determining where it is bounded by the bolt and nut triangle. This, in turn, will reduce the potential for error in the contact point location. Moreover, note that it is of primary interest to minimize the number of contact pairs involved in a contact so as to eliminate the potential for error.

The following steps summarize how we approximate the contact point (Fig. 4):

1. Derive an equation of a line that defines each boundary of the bolt triangle.
2. Enumerate where line **l**, intersects the bolt triangle (b_{c1}, b_{c2}, b_{c3}).
3. Check and identify which two of the three points are bounded by the bolt triangle.
4. Derive an equation of a line that defines each boundary of the nut triangle.
5. Enumerate where line **l**, intersects the nut triangle (n_{c1}, n_{c2}, n_{c3}).
6. Check and identify which two of the three points are bounded by the nut triangle.
7. Determine if any of the nut points fall within the boundary of the bolt triangle.
8. Extract the endpoints of the line segment.
9. Calculate the midpoint, and repeat steps 1–8 for next contact pair.
10. Average midpoints from each contact pair.

All of these calculations are necessary, since we do not have prior knowledge of the order of the intersection points (b_{c1}, b_{c2}, b_{c3}). In the first contact situation, the four ordered pairs of the bolt and nut intersection points produce four possible ar-

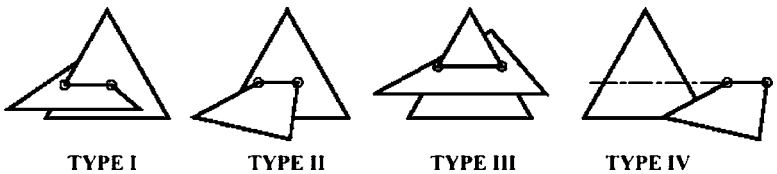

Fig. 3 Types of bolt and nut triangle intersection

Table 1 Angles for Type I intersection

	θ_0^1	θ_0^2	θ_1^1	θ_1^2
$(n_{c2}, b_{c1}, n_{c3}, b_{c2})$	π	0	0	0
$(n_{c3}, b_{c1}, n_{c2}, b_{c2})$	0	π	0	0
$(n_{c2}, b_{c2}, n_{c3}, b_{c1})$	0	0	π	0
$(n_{c3}, b_{c2}, n_{c2}, b_{c1})$	0	0	0	π

Table 3 Angles for Type III intersection

	θ_0^1	θ_0^2	θ_1^1	θ_1^2
$(n_{c2}, n_{c3}, b_{c1}, b_{c2})$	π	0	0	π
$(n_{c2}, n_{c3}, b_{c2}, b_{c1})$	π	0	0	π
$(n_{c3}, n_{c2}, b_{c2}, b_{c1})$	0	π	π	0
$(n_{c3}, n_{c2}, b_{c1}, b_{c2})$	0	π	π	0

rangements of the angle between them as shown in Table 1:

Thus, the intersection between the bolt and nut will fall into the first type provided that the angle between the respective vectors matches one line in the table above. If not, then the angular results are compared with the next intersection type. In addition to the angular check, the magnitudes of the vectors (shown in steps 1–3 and 5–7) are compared in order to verify that the intersection point falls within the plane of the bolt triangle. If the nut intersection point does not fall within the plane of the triangle, then either the fourth or fifth intersection type will define the resulting line segment.

In the second contact situation, the values of the angles are all zero. The third contact situation is detailed in Table 2, and the fourth contact situation is outlined in Table 3.

Before defining the multiple contact state models, we will begin with a brief review of coordinate system transformations since this technique is required to understand the progression of the bolt from the initial to the final contact state.

5 Possible Contact States

The contact analysis sets the nut coordinate axes as the fixed reference frame and the bolt coordinate system as the moving frame. The bolt axes are located in space via three rotations and one translation (Fig. 5). For this analysis, the translational errors in the X_h and Y_h directions are assumed to be zero. The rotations are conducted by rotating about the Z_s-axis an amount ϕ, rotating about the Y_s-axis an amount β, and finally rotating about the X_s-axis an amount α. These three angles will herein be referred to as the phase, pitch, and roll, respectively. Several contact states are possible as roll and pitch rotations are completed during insertion of the bolt into the nut. These states are outlined in Fig. 6, and each type will be discussed below.

Case 1: Positive Roll, Zero Pitch

The bolt contacts the surface of the nut for a majority of phase rotation. A positive rotation about the X_n-axis causes the crest of the bolt to be the leading edge. Since the radius of the bolt is a maximum at this location, the contact state will primarily occur at the surface of the nut. As the angular position of the bolt changes about the Z_n-axis, the contacting surface of the bolt changes from the positive crest fillet, to the crest, and then on to the negative crest fillet. The clearance window is defined as the area where the bolt radius is always less than the nut radius after its angular orientation and translational positions are given. This ledge as shown in the figure is defined as the *negative root fillet*, because the radius of the nut decreases when measured along the positive Z_n-axis. Eventually, the bolt will enter the clearance window, and it will undergo a negative vertical shift.

At this point, the contact switches from the negative crest fillet to the positive crest fillet because this surface travels the minimum distance to the nut. For the next several degrees, the bolt raises out of the nut by a consistent rate of change, which is dependent on the pitch p of the thread, as seen in Eq. (1). Figure 7 indicates the change in depth of the bolt as it is rotated about the nut. These are the numerical results associated with the tessellated model. Although the negative vertical shift is shown, some numerical artifacts exist just before and after the bolt falls in phase. At 1 deg of roll, the vertical position of the bolt shows a maximum variability of 45 μin., while at 4 deg the magnitude of the artifact increases to 193 μin. However, manual cross section analysis of the computer model shows that the bolt cannot have a contact below the surface in these regions. It was discovered that the amount of vertical shift varies nonlinearly with the roll angle. A larger roll angle results in an increased clearance window, therefore allowing the bolt to drop deeper in the nut. Corresponding to the interacting surfaces described above, we found that the resultant normal vectors do not vary significantly except at the very narrow drop range.

Table 2 Angles for Type III intersection

	θ_0^1	θ_0^2	θ_1^1	θ_1^2
$(n_{c2}, b_{c1}, b_{c2}, n_{c3})$	π	0	π	0
$(n_{c2}, b_{c2}, b_{c1}, n_{c3})$	0	π	0	π
$(n_{c3}, b_{c2}, b_{c1}, n_{c2})$	0	π	0	π
$(n_{c3}, b_{c1}, b_{c2}, n_{c2})$	π	0	π	0

The right hand side of Fig. 6 shows why the depth change in Fig. 7 is not a sawtooth, but a few words of explanation are needed. The contact surfaces constantly change with phase angle from the root to the crest so that the corresponding helices effectively cancel out any vertical motion. When the contacts shift to the fillets, in all cases no more than about 60 deg range of phase angle, this effect vanishes. The minor sawtooth patterns are artifacts from the surface tessellation.

Case 2: Negative Roll, Zero Pitch

This configuration begins with the negative flank as the leading edge and a two-point contact at the surface of the nut, but immediately returns to a one point contact state after 1 deg of rotation about Z_n. As the bolt rotates counter-clockwise, the contacting radius transitions from the negative flank to the negative root fillet, while the nut radius also transitions from the negative flank to the negative root fillet. The negative root fillet of the nut acts as the ledge restricting the bolt from contacting a point beneath the surface. Once the bolt enters the clearance window, the surfaces in contact change in a similar fashion as described in case 1. However, the vertical transition is subtle because the surface that travels the minimum distance is the positive root fillet. It appears that the contacts "switch" positions when one examines a vector plot

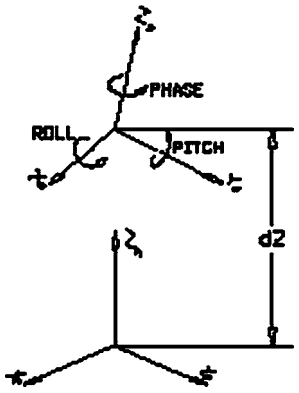

Fig. 5 Definition of rotation angles

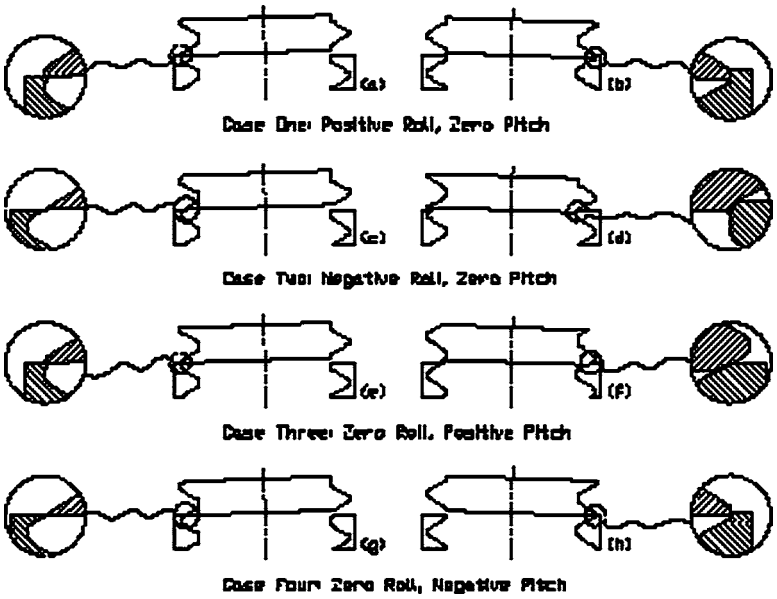

Fig. 6 Possible contact state configurations

of the contact normals [4]. The contact state maintains continuity by seeking a contact point on the positive root fillet below the surface.

The minimum Z_b-coordinate of the triangles that come into contact represents a depth that is larger than theoretically possible (Fig. 8). Although it accurately depicts when the bolt aligns with the nut, the value that is extracted for the depth actually occurs below the contact point. It is for this reason that the depth chart shows a large variability with an increasing roll angle. Therefore, these charts will only be used to verify where the clearance window begins and ends.

Case 3: Zero Roll, Positive Pitch

This case begins like case 2 but it does not start with a two point contact situation. Again, as the bolt is rotated about the Z_n-axis, the contact point is located between the negative crest fillet of the bolt and nut, respectively. Once the bolt radius enters the clearance window the contact point advances approximately 90 deg to the positive flank of the bolt and nut, respectively (Fig. 9). The bolt drops a minimal distance and the contact point rapidly returns to the surface within several degrees of phase. This configuration has the same discrepancies in the depth chart as in the previous case, but it still accurately indicates the location of the contact point transition.

Case 4: Zero Roll, Negative Pitch

As shown in the depth chart and the vector plot (not shown here) the contacts occur in a mirror image of case 3 (Fig. 10). Once the bolt enters the clearance window, the contact point below the surface occurs between the crest of the bolt and the positive crest fillet of the nut. In this case, the depth can be accurately determined by extracting the minimum Z_b-coordinate of the contacting triangles. After analysis of the four possible contact states, models are derived to identify the contact state as the bolt moves vertically downward to contact the nut. This process is detailed in the next section.

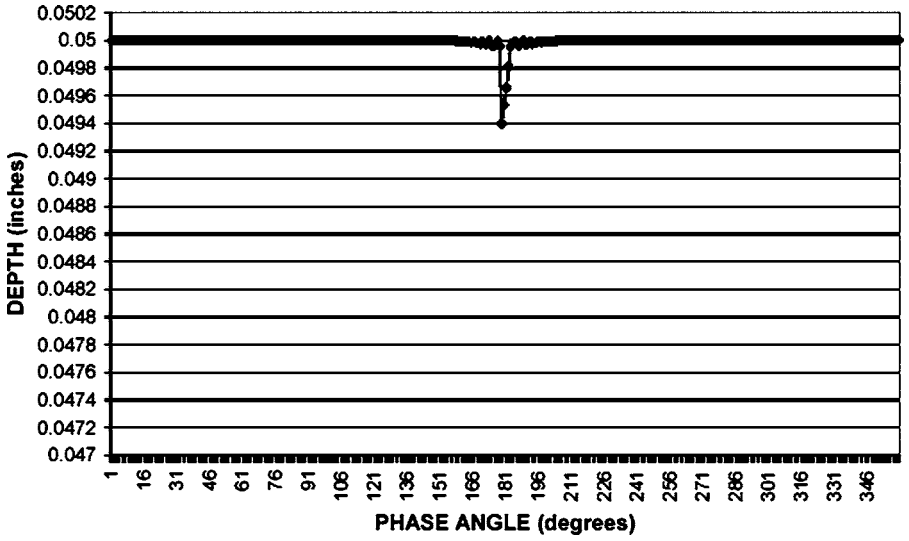

Fig. 7 Depth change as a function of phase rotation for case 1

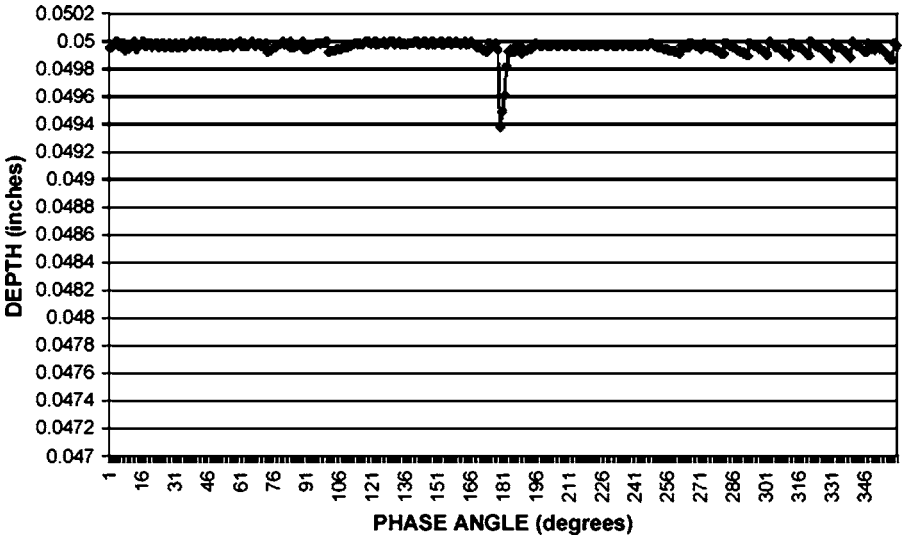

Fig. 8 Depth change as a function of phase rotation for case 2

6 Contact State Models

6.1 First Contact State Model. The data files of the bolt and nut are exported from PRO/ENGINEER sharing the same reference frame. This reference frame will be referred to as the "fixed" frame. All the vertices of the bolt undergo a transformation that orients and translates each coordinate in space. The bolt is then translated along the *Z*-axis of the fixed frame in a series of regressing steps of finer adjustment until contact with the nut is made, since it is of primary interest to cause a contact with the least amount of penetration (smallest number of contact pairs). Once the final move is made, at a selected value of 10 μin., the contact pairs are sent to the contact location subroutine. Figure 11 shows the orientation of the reference frames, and the transformation between them once the first contact point ($\mathbf{CP_0}$) is obtained.

To make the subsequent manipulation of such transformations more readable, a cyclic graph approach will be employed, as shown in Fig. 16, below.

The vector **u** locates the contact point $\mathbf{CP_0}$, and the vector **t** locates the origin of the bolt reference frame; both of which are measured with respect to the fixed reference frame. The vector **s** locates the contact point as measured in the bolt reference frame. The vertices of the bolt are transformed to the fixed frame via Eq. (2):

$$P_F = {}^b_F T^{-1} P_b \tag{2}$$

The transformation involves a 3-2-1 rotation and a translation; it is defined as [13]:

$${}^b_F T = \mathrm{Rot}_Z(\phi)\mathrm{Rot}_Y(\beta)\mathrm{Rot}_X(\alpha)\mathrm{Trans}(t) \tag{3}$$

In this notation, $\mathrm{Rot}_z(\phi)$ indicates a positive rotation of ϕ deg about the *Z*-axis, and Trans(**t**) represents a translation through the vector **t**. Note that α, β, and ϕ are given because the orientation of the bolt is known *a priori*, and the value of the translation vector (**t**) is determined numerically through the series of regressing steps mentioned earlier. Now, the contact point as viewed in the bolt frame can easily be calculated through the following homogeneous transformation:

$$P_b = {}^b_F T P_F \tag{4}$$

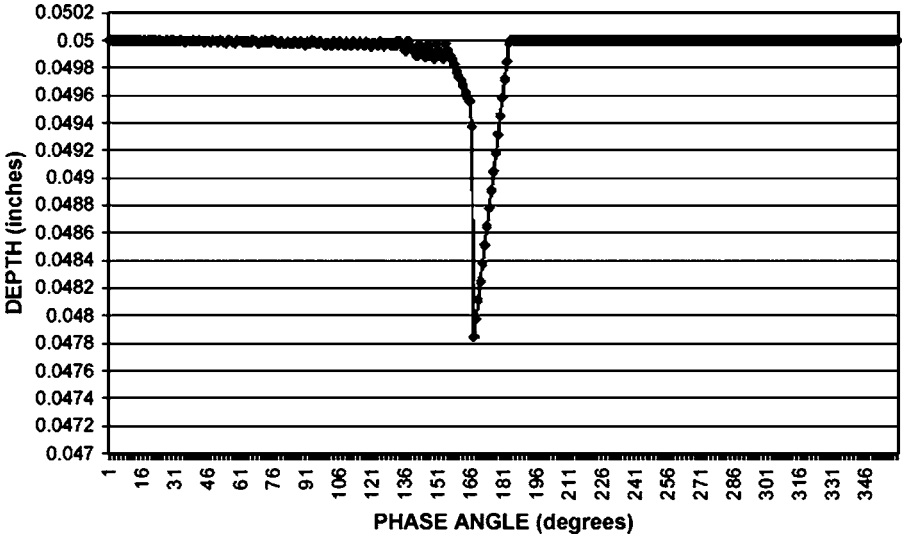

Fig. 9 Depth change as a function of phase rotation for case 3

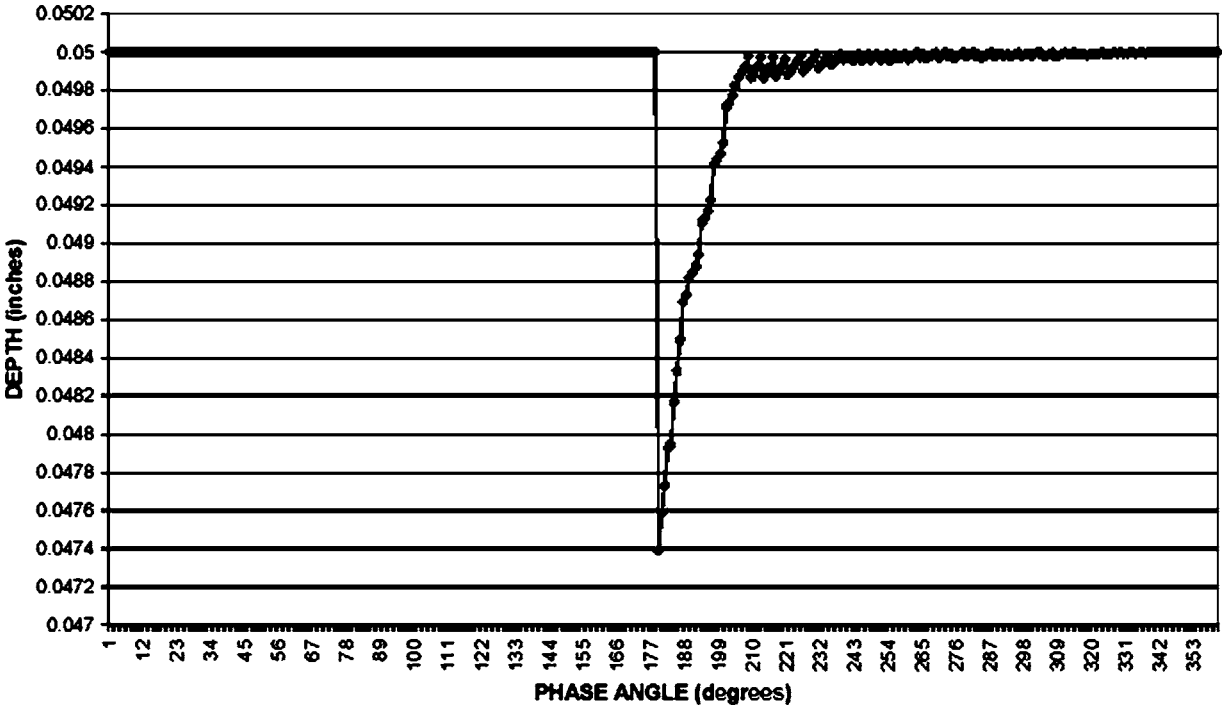

Fig. 10 Depth change as a function of phase rotation for case 4

This is useful because the parametric equation that defines the cross section of the bolt at the contact can only be utilized once the contact point in the bolt reference frame is known.

6.2 Second Contact State Model. Once the first contact point is obtained, a new reference frame $\mathbf{C_0}$ is created at the location of the contact point $\mathbf{CP_0}$. This is done because the collision detection library RAPID needs to start with both tessellated models sharing the same reference frame. Thus, the bolt triangles maintain the first contact point configuration prior to a subsequent rotation about the *X*-axis of the $\mathbf{C_0}$ frame. The actual contact locations are stored in memory and converted back to the fixed reference frame so the user has knowledge of where the contacts occurred with reference to the actual position of the bolt and nut. The *X*-axis of the $\mathbf{C_0}$ frame is aligned with a vector drawn tangent to the nut surface at the contact location. The bolt and nut vertices will be rotated about this *X*-axis until the second contact point is obtained (Fig. 12).

Before commencing with a rotation about the x-axis of the $\mathbf{C_0}$ frame, the bolt and nut vertices must be transformed by the following matrix equations:

$$P_{\mathbf{C_0}} = {}^{\mathbf{C_0}}_{F}T\,T_F^b\,T^{-1}P_b, \tag{5a}$$

$$P_{\mathbf{C_0}} = {}^{\mathbf{C_0}}_{F}TP_n, \tag{5b}$$

where

$${}^{\mathbf{C_0}}_{F}T = \mathrm{Rot}_z(-\delta_1)\mathrm{Rot}(-\delta_2)\mathrm{Trans}(-u). \tag{6}$$

Angles δ_1 and δ_2 are calculated from the direction cosines of the vector tangent to the surface of the nut at the contact point and are represented in the fixed reference frame. Figure 13 depicts the two-step process of transforming the X_F-axis to a general orientation of a vector tangent to the nut surface.

The fixed frame is rotated about the Z_F-axis first by an amount δ_1. Then the new fixed frame (denoted by a prime) is rotated about the Y'_F-axis by an amount δ_2. The formulae for calculating δ_1 and δ_2 are given below:

$$\delta_1 = a\cos\left[\frac{\theta_x}{\sin(a\cos\theta_z)}\right] \tag{7a}$$

$$\delta_2 = a\cos(\theta_z) - \left(\frac{\pi}{2}\right) \tag{7b}$$

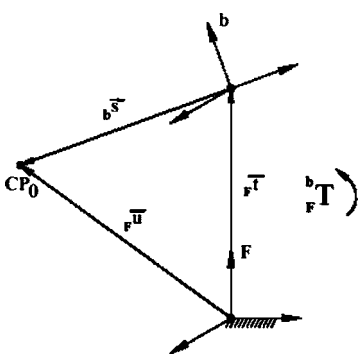

Fig. 11 First contact state model

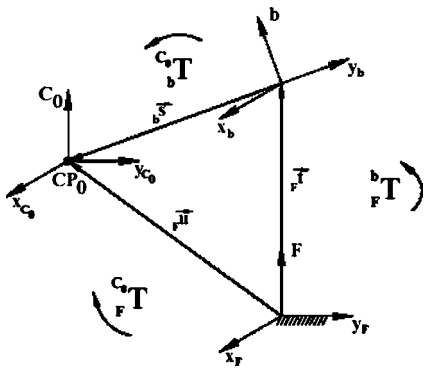

Fig. 12 Second contact state model

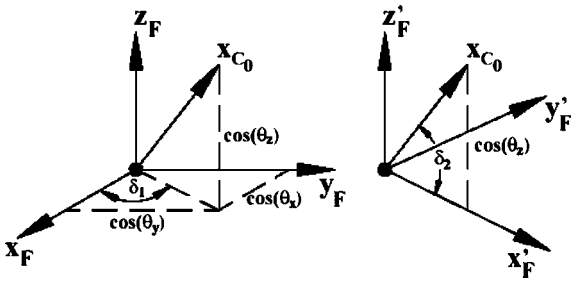

Fig. 13 Vector rotation angles

Note that θ_x and θ_z are the direction cosines of the tangent vector expressed in radians, since the vector tangent to the surface of the nut at the contact point is of unit magnitude. The transformation that orients the bolt frame with the $\mathbf{C_0}$ frame follows a similar derivation. Here, the X_B-axis must be aligned with the $X_{\mathbf{C_0}}$-axis via two successive rotations, ψ_1 and ψ_2. However, the direction cosines of the vector tangent to the nut surface must be expressed in the bolt frame prior to the computation of these angles.

$$ {}^{\mathbf{C_0}}_{b}T = \mathrm{Rot}_z(-\psi_1)\mathrm{Rot}_y(-\psi_2)\mathrm{Trans}(-s) \tag{8} $$

$$ \psi_1 = a\cos\left[\frac{\theta_x^b}{\sin(a\cos\theta_z^b)}\right] \tag{9a} $$

with

$$ \psi_2 = a\cos(\theta_z^b) - \left(\frac{\pi}{2}\right). \tag{9b} $$

At this point, the bolt is rotated about the X-axis of the $\mathbf{C_0}$ frame until the second contact point is obtained. The direction of rotation is negative, because the vector tangent to the surface of the nut is directed counter-clockwise, and the assembly force is acting along the negative azimuth axis of the bolt. Subsequently, a negative rotation about this axis will rotate the bolt towards the nut surface. Figure 14 depicts the position of the bolt frame once it obtains the second contact point $\mathbf{CP_1}$.

The transformation that carries the bolt to the second contact state is simply comprised of a rotation about the $X_{\mathbf{C_0}}$ axis:

$$ {}^{\mathbf{C_1}}_{\mathbf{C_0}}T = \mathrm{Rot}_{X_{\mathbf{C_0}}}(\lambda) \tag{10} $$

The advent of the second contact point provides a more constrained situation, as now the bolt has a maximum of two degrees of freedom provided it still maintains both contact points. Once the bolt has achieved this situation, a new model of the nut and bolt must be created as observed from a new reference frame defined by the contact points. At all times the contact states are

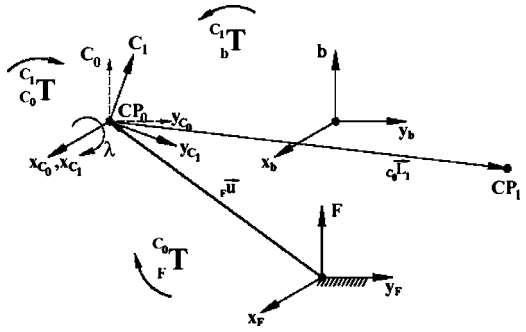

Fig. 14 Coordinate frames at two-point contact

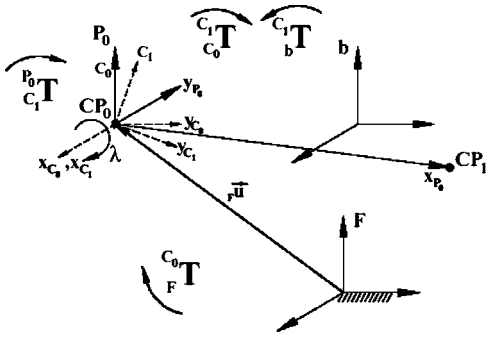

Fig. 15 Third contact state model

validated as being quasi-stable with respect to an elastic support, such as an RCC.

6.3 Third Contact State Model. Once again, an additional reference frame will be established at the initial contact point $\mathbf{CP_0}$, but the X-axis of this coordinate system will be defined by a vector drawn from the first to the second contact point (Fig. 15).

The transformation from the fixed frame to the $\mathbf{P_0}$ frame will follow a similar derivation for the transformation from the fixed frame to the $\mathbf{C_0}$ frame. However, in this case, the transformation will occur in several steps. The first step, already known, is the transformation of the fixed frame to the $\mathbf{C_0}$ frame. The second step is the transformation from the $\mathbf{C_0}$ frame to the $\mathbf{P_0}$ frame. Again, there are two rotations that line up the $\mathbf{C_0}$ coordinate axes with a general vector in space. The two rotations are:

$$ \theta_{P1} = a\cos\left[\frac{\theta_x^P}{\sin[a\cos(\theta_z^P)]}\right] \tag{11a} $$

$$ \theta_{P2} = a\cos(\theta_z^P) - \left(\frac{\pi}{2}\right) \tag{11b} $$

θ_x^p and θ_z^p are direction cosines of the $X_{\mathbf{P_0}}$-axis as measured from the $\mathbf{C_0}$ frame. Now, the transformation follows directly from the previous derivation:

$$ {}^{\mathbf{P_0}}_{\mathbf{C_0}}T = \mathrm{Rot}_z(-\theta_{P_1})\mathrm{Rot}_y(-\theta_{P_2}) \tag{12} $$

Given a set of coordinates in the fixed frame, one can transform them to the $\mathbf{P_0}$ frame via the following calculation:

$$ P_{\mathbf{P_0}} = {}^{\mathbf{P_0}}_{\mathbf{C_0}}T\,{}^{\mathbf{C_0}}_{F}T P_F \tag{13} $$

The transformation equation for coordinates initially given in the bolt frame is somewhat more complicated. Recall that the bolt vertices begin by being represented in the fixed frame. The vertices must be transformed to the current location of the bolt coordinate system, so they are transformed to the initial contact configuration first (such that the bolt coordinate system at the moment of initial contact is viewed from the fixed reference frame). Then they are transformed from the fixed to the $\mathbf{C_1}$ frame, followed by an inverse transformation to record the second contact configuration of the bolt (the moment when the bolt obtains two contact points) as represented in the $\mathbf{C_0}$ frame. Finally, the bolt vertices are transformed from the $\mathbf{C_0}$ to the $\mathbf{P_0}$ frame. The cyclic representation of the transformations involved is shown in Fig. 16.

The entire homogeneous transformation is shown in the equation below:

$$ P_{\mathbf{P_0}} = {}^{\mathbf{P_0}}_{\mathbf{C_0}}T\,{}^{\mathbf{C_1}}_{\mathbf{C_0}}T^{-1}\,{}^{\mathbf{C_1}}_{F}T\,{}^{b}_{F}T^{-1}P_b \tag{14} $$

Unlike the second contact point analysis, when the direction of rotation was known, the direction of rotation about the X_P-axis must be determined. The X-Y plane of the $\mathbf{P_0}$ frame is assumed to be parallel to the X-Y plane of the fixed frame, since a majority of

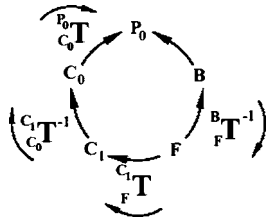

Fig. 16 Cyclic diagram for third contact state model

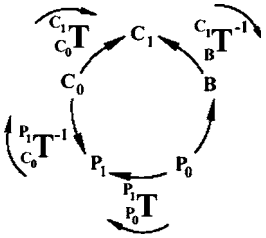

Fig. 18 Cyclic diagram to convert to bolt reference frame

the contact points will occur at or near the surface. Hence, the fixed frame is simulated at the surface of the nut while the direction of rotation about the X_P-axis is determined. The enumeration of the quadrant location of $\mathbf{CP_0}$ and $\mathbf{CP_1}$, the determination of whether the X_P-axis intersects the positive or negative X_F-axis and whether the slope of the X_P-axis is positive or negative, will determine the direction of rotation. All of these parameters are measured with respect to the fixed reference frame.

For each of the quadrants that $\mathbf{CP_0}$ has the potential to occur in, there is one configuration that is geometrically impossible. In the previous example, it is geometrically impossible for $\mathbf{CP_0}$ to occur in quadrant one, the X_P-axis to intersect the negative X_F-axis, and for the slope of the X_P-axis to be negative.

At the moment the bolt obtains a third contact point with the nut, it is assumed to have a stable configuration. At this point the motion of the bolt is complete, and the critical contact data can be exported into a data file. Figure 17 depicts the coordinate systems at the moment the third contact point ($\mathbf{CP_2}$) is obtained.

The final transformation that pivots the bolt into the third contact point is:

$$\overset{\mathbf{P_1}}{\mathbf{P_0}}T = \mathrm{Rot}_x(-\zeta) \tag{15}$$

The series of transformations that convert a set of contact coordinates as measured in the $\mathbf{P_0}$ to the fixed frame is shown below:

$$P_F = \overset{\mathbf{C_0}}{F}T^{-1}\overset{\mathbf{P_0}}{\mathbf{C_0}}T^{-1}P_{\mathbf{P_0}} \tag{16}$$

However, knowledge of where the contacts occurred as measured from the bolt frame is required to ascertain the appropriate parametric equation. Since the models of the bolt and nut were recreated in the $\mathbf{P_0}$ frame, any contact point will be represented by this coordinate system. Hence, the coordinates must be converted from the $\mathbf{P_0}$ frame to the bolt frame. This more complicated procedure begins with a transformation from the $\mathbf{P_0}$ frame to the $\mathbf{P_1}$ frame, followed by an inverse transformation that carries the coordinates from the $\mathbf{P_1}$ to the $\mathbf{C_0}$ frame. At this point the vertices are transformed from the $\mathbf{C_0}$ frame to the $\mathbf{C_1}$ frame, followed by another inverse transformation that converts the vertices from the $\mathbf{C_1}$ frame back to the bolt frame. A cyclic representation of the transformations involved in the conversion from the $\mathbf{P_0}$ to the bolt frame is shown in Fig. 18.

The entire transformation is shown in Eq. (17):

$$P_b = \overset{\mathbf{C_1}}{b}T^{-1}\overset{\mathbf{P_1}}{\mathbf{C_0}}T\overset{\mathbf{P_1}}{\mathbf{C_0}}T^{-1}\overset{\mathbf{P_1}}{\mathbf{P_0}}TP_{\mathbf{P_0}}. \tag{17}$$

Note that the transformations from the bolt to the $\mathbf{C_1}$ frame and from the $\mathbf{C_0}$ to the $\mathbf{P_1}$ frame are equivalent to the transformations from the bolt to the $\mathbf{C_0}$ frame and from the $\mathbf{C_0}$ to the $\mathbf{P_0}$ frame, respectively.

The direction of the contact normal is critical in the determination of the potential for jamming and/or wedging. During a threaded assembly, it is possible to determine the common normal between two helically swept surfaces through the use of vectors tangent to the bolt and nut. The following section outlines the technique involved in the determination of a common normal at a contact point between the bolt and nut.

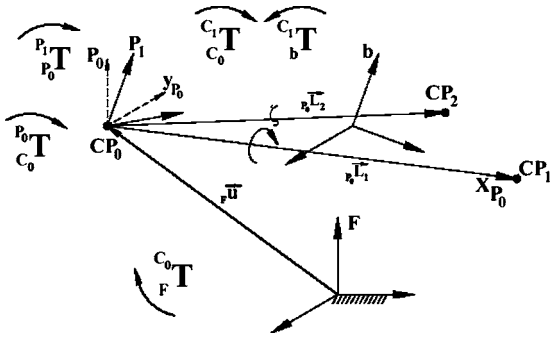

Fig. 17 Coordinate frames at three-point contact

7 Spatial Contacts from Discretized Orientation Errors

Recall that the threaded assembly may be completed by the conventional heuristic of rotating the bolt counter-clockwise until a "snap" is heard. The "snap" results from a sudden change in the height of the bolt and occurs when the bolt is in phase with the nut. From this point it is known that any clockwise rotation results in a successful assembly provided that the orientation is maintained. By utilizing the contact state models derived in the previous section, we conducted an exhaustive test sequence simulating this heuristic to ascertain the contact locations throughout a counter-clockwise rotation of the bolt.

The initial approach of the bolt has six degrees of freedom, three rotations (roll, pitch, and phase) and three translations (horizontal, vertical, and azimuth), resulting in a multitude of infinities. One way to reduce the number of free choices during the initial approach is to develop a pre-alignment strategy. An example of this is the azimuth rotation strategy as discussed by Sturges [1,2] that preconditions the constraint network for prismatic peg insertion. In our case, the bolt shall be considered as having two rotational freedoms (roll, α, and pitch, β) over the range −4, 0, and +4 deg, as this is the extent of expected elastic compensation for an RCC. Thus, the bolt can be pre-aligned eight different ways based on the rotational degrees of freedom: $+\alpha$ only; $+\beta$ only; $-\alpha$ only; $-\beta$ only; $+\alpha$ and $+\beta$; $+\alpha$ and $-\beta$; $-\alpha$ and $+\beta$; $-\alpha$ and $-\beta$. For this analysis, it will be assumed that the translation errors in the vertical and horizontal directions (X- and Y-axes) are corrected by the standard RCC. The azimuth translation (Z-axis) is constrained by the orientation of the bolt, as it is calculated once the bolt achieves its first contact. Hence the bolt will be positioned above the nut, and moved down the azimuth axis until RAPID detects a contact. Since the bolt will be rotated counter-clockwise, there are no restrictions on the phase angle ϕ, so it was discretized over one period (zero to 360) in steps of 5 deg, in order to determine the entire gamut of potential contact states. The complete set of motions involved in the contact analysis was numerically simulated by a supervisory code written in Microsoft Visual C++ and executed on a desktop workstation.

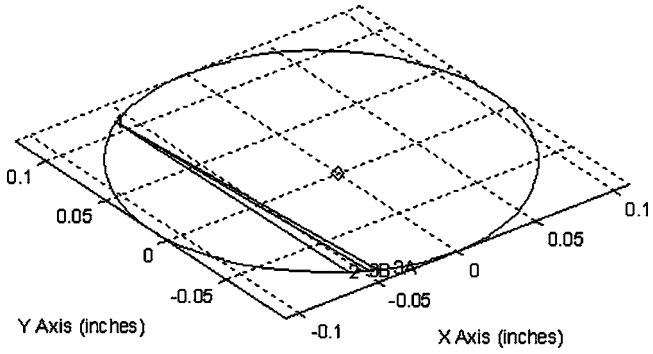

Fig. 19 Unstable contact point locations (α=4, β=0, ϕ=185)

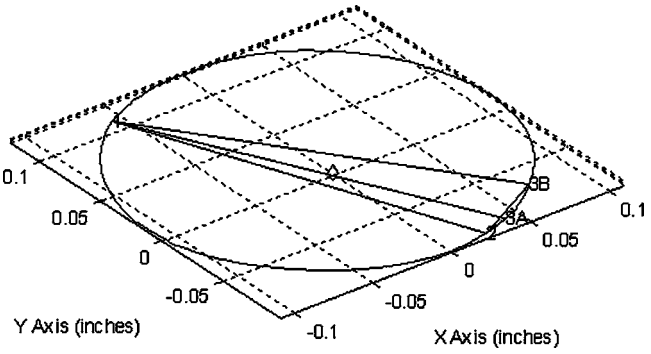

Fig. 20 Quasi-stable contact point locations (α=4, β=4, ϕ=235)

7.1 Contact State Analysis. In order to determine if there was excessive interference, the origin of the bolt reference frame at the two-point and three-point contact states needs to be recorded. If the origin of the bolt frame moved less then the amount that the bolt embedded in the nut, then we have an unstable case because we located a third contact point by doing something impossible (embedding a rigid body into another rigid body). If the origin of the bolt frame drops more than the amount that the bolt embeds in the nut, then this is a possible movement because the bolt is releasing its potential energy. Furthermore, the location of the pivot axis will determine the stability of the bolt at the second contact state. If the pivot axis crosses at or near the origin of the bolt, then we could have a special "quasi-stable" two-point contact case. Here, the axis passes close to the compliance center (origin of the bolt frame) at which point the moment due to the applied load is nearly negligible. If the axis is far away from the origin of the bolt, then the code is unable to determine where the third contact point is because the pivot axis is *rolling* on the surface thereby producing an unstable contact state. A *rolling* axis is defined as acquiring more triangles at one or both of the original points once rotation about the pivot axis commences. Therefore, the output file was analyzed to determine whether the computed contact information was two-point unstable, two-point quasi-stable, or three-point stable throughout each of the eight approaches.

7.1.1 Unstable Two-Point Contact State. Figure 19 depicts four contact points labeled 1, 2, 3A, and 3B. Points 1 and 2 define the endpoints of the pivot axis, or the *X*-axis of the $\mathbf{P_0}$ frame. The code simulates a rotation of the bolt about the pivot axis until RAPID returns (and the code categorizes) three distinct contact states. In a majority of the test runs, it was found that the third contact point was only obtained by embedding itself into the nut, thereby producing a discontinuity in the contact pair output. This condition is an example of an unstable state for the given orientation.

The diamond in the center of the chart is the location of the bolt origin when the third contact state is reached. The circular object is the interior edge of the planar cross section of the nut. The swath of embedment is pictorially shown by the close proximity of points 3A and 3B. Here, the code detected a discontinuity between points 2 and 3A, so it stopped rotating the bolt about the pivot axis and returned a series of contact pairs. In this case, it is determined that the bolt is unstable, because the origin of the bolt frame moved less than the amount embedded in the nut. The origin of the bolt frame moved from 0.047 to 0.046 in. (1.19 to 1.17 mm), or a displacement of 0.001 in. (0.03 mm). However, the depth of embedment was found to be 0.004 in. (0.10 mm), which is greater than the movement of the bolt reference frame, therefore we have an unstable case.

7.1.2 Quasi-Stable Two-Point Contact State. A "quasi-stable" two-point case is also present when approaching the nut with a positive rotation about the roll and pitch axes (Fig. 20). Here the bolt reference frame dropped 0.0045 in. (0.11 mm) but the largest amount of interference was 0.0013 in. (0.03 mm), therefore, the bolt released some potential energy as it moved down the azimuth axis of the fixed reference frame. Although only two contact points are present, the pivot axis passes near the origin of the bolt reference frame, thereby providing the potential for stability with an appropriately applied force.

Once again, the diamond in the center of the chart signifies the origin of the bolt reference frame, and points 1 and 2 represent the endpoints of the pivot axis. However, the code continued to rotate until it obtained a swath of triangles that begin with point 3A and end with 3B, since it is unable to decipher a quasi-stable contact configuration.

7.1.3 Stable Three-Point Contact State. An example of a stable three-point contact case is shown in Fig. 21. Here, the number of contact pairs at each of the distinct contact points is minimized (4 pairs each). Moreover, the bolt did not embed itself into the nut as it pivoted about the axis defined by points 1 and 2. The origin of the bolt frame dropped slightly as it rotated about the $X_{\mathbf{P_0}}$-axis; however, all three contact points occurred at the surface of the nut which means that the two solid bodies did not interface with one another. This type of result was interspersed throughout each of the approaches, but it occurred the least number of times.

7.2 Expansion to All Rotational States. The derived parametric equations can be used without modification to create a full spectrum of maps at any point in the history of a threaded assembly operation. For the two-dimensional case, the contact points were calculated once the contacting surface regions were identified (details in [11]). Surface regions are shown here with respect to the phase angle graphically as annuli in Fig. 22.

In the three-dimensional case, errors in rotation about the *X*- and *Y*-axes of the bolt reference frame are permitted. This creates

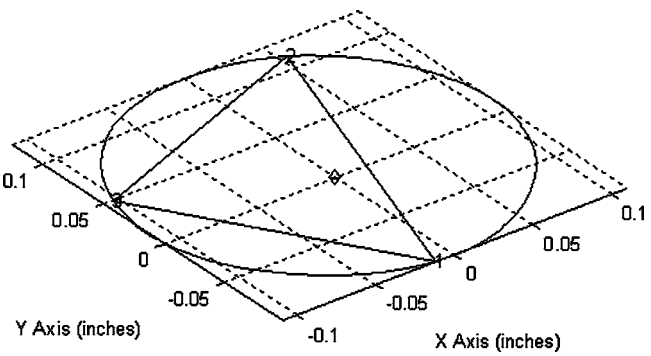

Fig. 21 Stable contact point locations (α=−4, β=0, ϕ=131)

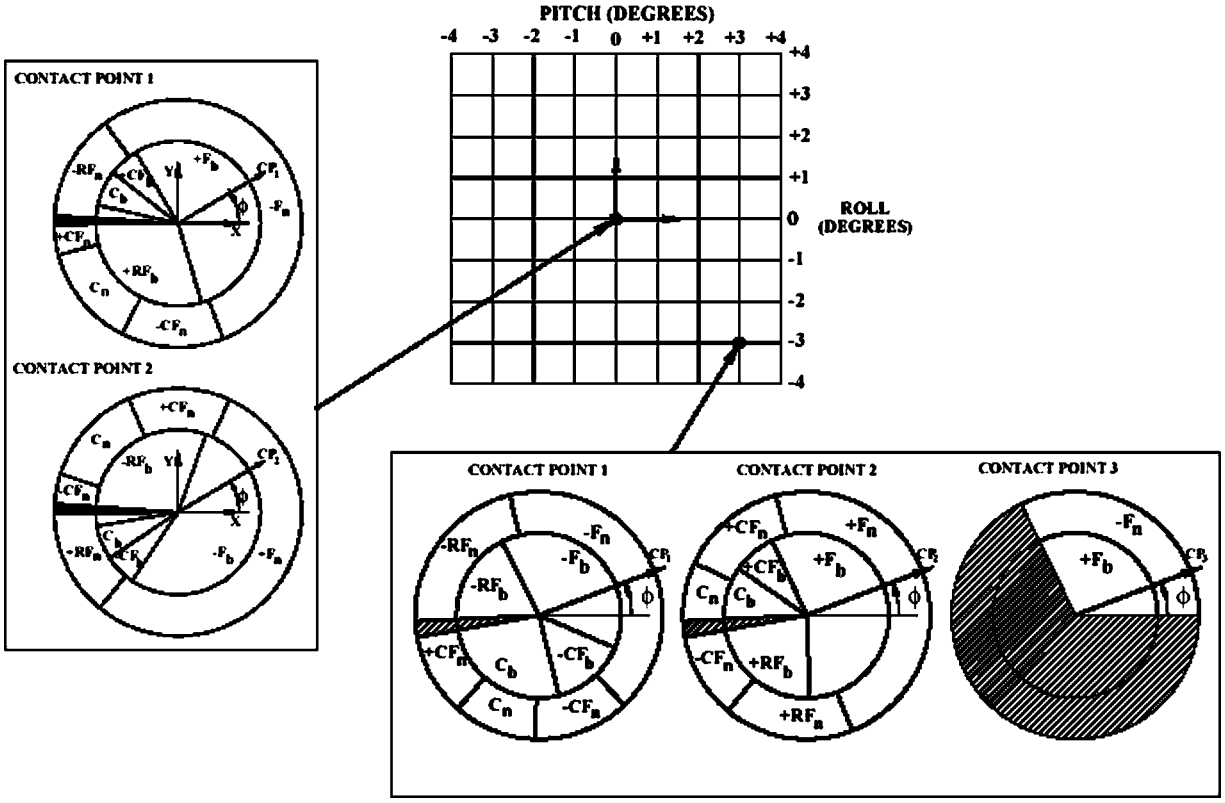

Fig. 22 Relation of contact states to all angular conditions

the opportunity for out-of-plane contacts, where each contact will have its own annulus describing the surface regions in contact. However, the annulus representing the range of contact must be modified to represent the parametric equations of the bolt cross section at the moment a third contact point is obtained, or when the bolt is no longer parallel to the nut surface. Figure 22 shows the expansion of the two-dimensional analysis into the three-dimensional contact analysis. For our purposes, values of roll and pitch were calculated at every 1-deg from −4 to +4 deg. Thus, our three-dimensional analysis covers 81 cases of thread mating contacts for every possible phase angle between the nut and bolt. For example, Fig. 22 shows the contact states for a bolt with rotational errors of −3 deg roll and +3 deg pitch. The contact regions, once the third contact is obtained, are shown below the grid that represents the gamut of orientation errors.

In this way, 81 potential orientations are investigated, each of which has its own set of contact points. This amount of variation constitutes a library that comprises all the contact states. From this library, the user will be able to correlate a contact state history, and develop a constraint network that permits successful assembly. The choice and number of grid points and phase angles used in this analysis convince us, by exhaustive examination, that there are no other possible contact states.

8 Conclusions

The technique used to locate the contact point began with the tessellation of one pitch of a #1/4-20 UNC thread, both internal and external. Tessellation was necessary since we utilized a collision detection library RAPID, which required the solid bodies to be stored in memory as a series of triangles. During a collision, spatial geometry was used to locate an approximate contact point. Here, given a contact pair, the coordinates of the endpoints of a line segment created by the planar intersection of a bolt and nut triangle were enumerated through vector geometry. The midpoint of the line segment for each contact pair was averaged to produce an approximate location of the contact point. The minimum number of triangles was required to reduce the variation in position due to tessellation, so the bolt was dropped onto the nut in a series of iterations ending with 1 μin. (25.4×10^{-9} m) adjustments.

Since the insertion force is assumed to be acting through the origin of the bolt reference frame and parallel to the azimuth axis of the bolt, the first contact state was constructed that rotated the bolt about a tangent vector to the surface or edge of the nut until a second contact point was obtained. The advent of a second contact point presented a more constrained contact state since we are interested in maintaining both contacts; thus it was hypothesized that the bolt would rotate about an axis defined by the original two contact points. The appropriate transformations were derived and the models entered into RAPID such that it was possible to rotate about the pivot axis until a third contact point is enumerated.

In order to show that the hypothesis was true, we analyzed the depth of intersection of the bolt into the nut as well as the vertical movement of the origin of the bolt reference frame. This determined whether the bolt was releasing potential energy or embedding itself into the nut. The calculated results show three types of contact states returned by the program:

1. unstable two-point contact state
2. quasi-stable two-point contact state
3. stable three point contact state.

We investigated 81 potential orientations, each of which has its own set of contact points, which was described by a contact region disk. From this exhaustive examination, a contact state history can be found with certainty, and one may be able to develop a constraint network for passive compliance or algorithmic motion control.

Acknowledgments

This work was sponsored under NSF CISE/IRI, Grant No. GPG/NSF 95-27. Special thanks to Tiffany New for careful preparation of the manuscript.

Nomenclature

$\mathbf{C_i}$ = coordinate frame of contact points; $\mathbf{i}=0,1,2$

$\mathbf{CP_i}$ = bolt-nut contact points; $\mathbf{i}=0,1,2$; viewed in fixed frame

$\mathbf{P_i}$ = bolt-nut contact points; $\mathbf{i}=0,1,2$; viewed in bolt frame

${}^{b}_{F}T$ = homogeneous transformation of bolt coordinates into the fixed frame

b_{ci} = enumerated bolt contact

n_{ci} = enumerated nut contact

p = thread pitch

z = vertical displacement of bolt (with respect to nut)

α = roll angle

β = pitch angle

δ_i = roll or pitch angles of first contact point in fixed frame

θ_i = angles to identify direction cosines between coordinate frames

λ, ζ = roll or pitch angles of third contact point in fixed frame

ϕ = variable azimuth (yaw) angle

Ψ_i = roll or pitch angles of second contact point in fixed frame

References

[1] Sturges, R. H., and Laowattana, S., 1996, "Virtual Wedging in Three-Dimensional Peg Insertion Tasks," ASME J. Mech. Des., **118**, pp. 99–105.

[2] Sturges, R. H., and Laowattana, S., 1996, "Design of an Orthogonal Compliance for Polygonal Peg Insertion," ASME J. Mech. Des., **118**, pp. 106–114.

[3] Caine, M. E., 1985, "Chamferless Assembly of Rectangular Parts in Two and Three Dimensions," Master Thesis, Massachusetts Institute of Technology, Dept. of Mechanical Engineering.

[4] Wiedmann, S., and Sturges, R. H., 2000, "Kinematic Analysis Of Threaded Fastener Assembly In 3 Dimensions," Proc. ASME DETC'00, 10–13 Sept. 2000, Baltimore MD, CD-ROM: DETC2000/DFM.

[5] Savishchenko, V. M., and Bespalov, V. G., 1965, "The Orientation of Components for Automatic Assembly," Russ. Eng. J., **45**(5), pp. 50–52.

[6] Blaer, I. L., 1962, "Reliable Automatic Starting of Threaded Parts," Russ. Eng. J., **42**(12), pp. 32–34.

[7] Nicolson, E. J., and Fearing, R. S., Proc 91 IEEE RSJ Int. Workshop Intell Robots Syst IROS 91, 1992, pp. 30–37, Osaka, Japan.

[8] Nicolson, E. J., and Fearing, R. S., 1993, Proceedings-IEEE International Conference on Robotics and Automation, 1, pp. 484–490, Atlanta, GA.

[9] Diftler, M. A., and Walker, I. D., 1997, "Determining Alignment Between Threaded Parts Using Force and Position Data from a Robot Hand," Proceedings-IEEE International Conference on Robotics and Automation, **2**, pp. 1503–1510, Albuquerque, NM.

[10] Whitney, D. D., 2004, *Mechanical Assemblies: Their Design, Manufacture, and Role in Product Development*, Oxford University Press, New York.

[11] Wiedmann, S., 1999, "Kinematic Analysis Of Threaded Fastener Assembly In 3 Dimensions," M.S. Thesis, Virginia Tech Dept. of Mechanical Engineering.

[12] *Machinery's Handbook 24th ed.*, 1992, E. Oberg, F. D. Jones, H. L. Horton, H. H. Ryffel, R. E. Green, ed., Industrial Press Inc., New York, pp. 1520–1527.

[13] Crane III, C. D., and Duffy, J., 1998, *Kinematic Analysis of Robot Manipulators*, Cambridge University Press, New York, pp. 4–36.

[14] Gottschalk, S., Lin, M. C., and Manocha, D., 1996, "OBB-Tree: A Hierarchical Structure for Rapid Interference Detection," Technical Report TR96-013, Department of Computer Science, University of N. Carolina, Chapel Hill.